J. Am. Chem. Soc. **1996,** *118,* 13021−13030

Combined Static and Dynamic Density Functional Study of the Ti(IV) Constrained Geometry Catalyst (CpSiH$_2$NH)TiR$^+$. 1. Resting States and Chain Propagation

Tom K. Woo, Peter M. Margl, John C. W. Lohrenz,[†] Peter E. Blöchl,[‡] and Tom Ziegler*

Contribution from the Department of Chemistry, University of Calgary, 2500 University Drive, N.W., Calgary, Alberta, Canada T2N 1N4, MD-IM-FA Computational Chemistry, Bayer AG, Gebäude Q18, D-51368 Leverkusen, Germany, and Zurich Research Laboratory, IBM Research Division, Säumerstrasse 4, CH-8803 Rüschlikon, Switzerland

Received July 22, 1996. Revised Manuscript Received October 11, 1996[⊗]

Abstract: The resting state structure of the metallocene−alkyl cation, the coordination of the olefin to the preferred resting state structure, and the insertion process of the Ti-constrained geometry catalyst (CpSiH$_2$NH)TiR$^+$ have been studied with density functional theory. A combined static and dynamic approach has been utilized whereby "static" calculations of the stationary points on the potential surface are meshed with first principles Car−Parrinello molecular dynamics simulations. The first molecular dynamics simulation specifically addressing the structure of a metallocene−alkyl cation is presented showing rapid interconversion between γ- and β-agostic conformations. Complementary static calculations show a small energetic preference for a γ-agostic resting state. Coordination of the olefin to the Ti−alkyl resting state is likely to result in the formation of a β-agostic π-complex which is highly favored energetically over other π-complexes that may initially form. The whole propagation cycle was studied from π-complex to subsequent π-complex. The propagation barrier corresponds to the insertion process which was calculated to have a free energy barrier of $\Delta G^{\ddagger} = 24.3$ kJ/mol at 300 K. The initial β-agostic interactions which stabilize the π-complex are replaced by α-agostic bonds which stabilize the insertion transition state. A study of the back-side insertion process reveals that it may be competitive with the front-side insertion process.

1. Introduction

Metallocene-based catalyst technology is expected to revolutionize the immense polyolefin industry. It has been called the single most important development in catalyst technology since the discovery of Ziegler−Natta catalysts.[1,2] Recent developments in the metallocene technology itself are the mono-Cp "constrained-geometry catalysts" (CGC)[3−12] of the form (CpSiR$_2$NR)MX$_2$, where M = group 3,4 transition metal and X = CH$_3$, Cl (e.g., **1**). Constrained geometry catalyst systems were amongst the first single-site catalysts to have been commercialized,[13] and it is claimed that they produce a new family of linear polyethylenes which break the traditional rules of the structure−property−processibility relationships.[14] More specifically, CGCs produce polymers which possess desirable strength properties while still allowing for easy processibility. This exceptional characteristic of CGC polymers has been attributed to the inclusion of linear long chain branches into the polymer backbone, a feature not found in traditional commercial polyethylenes.

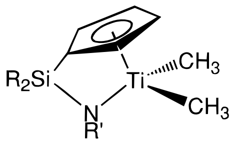

1

Except for the long chain branching the polymerization chemistry involving CGCs is expected to resemble that of conventional bis-Cp metallocenes, which have been extensively studied[15] both experimentally and theoretically. Only a handful of theoretical studies have specifically dealt with CGCs[16−19] including a recent Car−Parrinello molecular dynamics simulation by Iarlori *et al.*[19] In these studies only the insertion process of ethylene into the M−C bond of (CpSiH$_2$NH)MR$^+$, where R = methyl, was investigated. Since we are interested only in properties related to the "generic" features of the catalyst, we

---

[†] Bayer AG.

[‡] IBM Research Division.

[⊗] Abstract published in *Advance ACS Abstracts*, December 1, 1996.

(1) Sinclair, K. B. *Plast. Eng.* **1994** (Sept.), 19.

(2) Sinclair, K. B.; Wilson, R. B. *Chem. Ind.* **1994** (Nov.), 857.

(3) Stevens, J. C.; Timmers, F. J.; Wilson, D. R.; Schmidt, G. F.; Nickias, P. N.; Rosen, R. K.; Knight, G. W.; Lai, S. Eur. Pat. Appl. 90309496.9, August 30, 1990.

(4) Canich, J. A. M. Eu. Pat. App. 90309899.4, September 10, 1990.

(5) Devore, D. D.; Timmers, F. J.; Hasha, D. L.; Rosen, R. K.; Marks, T. J.; Deck, P. A.; Stern, C. L. *Organometallics* **1995**, *14*, 3132.

(6) Shipiro, P. J.; Cotter, W. D.; Schaefer, W. P.; Labinger, J. A.; Bercaw, J. E. *J. Am. Chem. Soc.* **1994**, *116*, 4623.

(7) Shipiro, P. J.; Bunel, E.; Schaefer, W. P.; Bercaw, J. E. *Organometallics* **1990**, *9*, 867.

(8) Lai, S.; Wilson, J. R.; Knight, G. W.; Stevens, J. C. U.S. Patent No. 5278272, January 11, 1994.

(9) Lai, S.; Wilson, J. R.; Knight, G. W.; Stevens, J. C.; Chum, P.-W. U.S. Patent No. 5272236, December 21, 1993.

(10) LaPointe, R. E. U.S. Patent No. 5321106, June 14, 1994.

(11) Nethamer, D. R.; Stevens, J. C. U.S. Patent No. 53507023, September 27, 1994.

(12) Nickias, P. N.; Devore, D. D.; Timmers, F. J.; Rosen, R. K.; Mussell, R. D. U.S. Patent No. 5347024, September 13, 1994.

(13) Lindsay, K. F. *Mod. Plast.* **1993** (Oct.), 82.

(14) Chum, P. S.; Kao, C. I.; Knight, G. W. *Plast. Eng.* **1995** (June), 21.

(15) Brintzinger, H. H.; Fischer, D.; Mülhaupt, R.; Rieger, B.; Waymouth, R. M. *Angew. Chem., Int. Ed. Engl.* **1995**, *34*, 1143.

(16) Woo, T. K.; Fan, L.; Ziegler, T. *Organometallics* **1994**, *13*, 2252.

(17) Woo, T. K.; Fan, L.; Ziegler, T. *Organometallics* **1994**, *13*, 432.

(18) Fan, L.; Harrison, D.; Woo, T. K.; Ziegler, T. *Organometallics* **1995**, *14*, 2018.

(19) Iarlori, S.; Buda, F.; Meier, R. J.; Van-DoreMaele, G. H. *J. Mol. Phys.* **1996**, *87*, 801.

S0002-7863(96)02525-5 CCC: $12.00

approximate the actual industrial catalyst (which carries a bulky substituent on the amido nitrogen) by its hydrogen-substituted analogue. Once the generic energy surface is known, perturbations caused by bulky substituents can be incorporated by less computationally expensive methods.

We present here the first part of a two-part density functional study of the whole propagation cycle, chain termination, and long chain branching for the Ti(IV) constrained geometry catalyst ($(CpSiH_2NH)TiR^+$). In the present part of the study we will examine the resting state of the Ti CGC−alkyl cation and the insertion process leading to chain propagation. In the following part[20] we will examine chain termination and long chain branching. To study these processes we have used a combined static and dynamic approach. On the one hand, the static method involves conventional electronic structure calculations to seek out stationary points on the potential energy surface. On the other hand, first-principles Car−Parrinello molecular dynamics simulations are used to sample a large number of conformations on those stretches of the potential surface which are related to the reactions under study.

2. Computational Details

The reported "static" density functional calculations were all carried out by the ADF program system version 1.1.3, developed by Baerends and others.[21−24] For the description of the electronic configuration (3s, 3p, 3d, 4s, and 4p) of titanium we used an uncontracted triple-ζ STO basis set.[25,26] For carbon (2s, 2p) and hydrogen (1s) a double-ζ STO basis, augmented with a single 3d or 2p polarization function respectively, was applied. No polarization functions were employed for carbon and hydrogen atoms on the Cp ring. The $1s^22s^22p^63s^2$ on Ti, the $1s^22s^22p^2$ on Si, and the $1s^2$ on C and N were assigned to the core and treated with the frozen core approximation.[27] In order to fit the molecular density and represent Coulomb and exchange potentials accurately a set of auxiliary s, p, d, f, and g STO functions,[28] centered on all nuclei was used in every SCF cycle. Energy differences were calculated by including the local exchange-correlation potential by Vosko[29] *et al*. with Becke's[30] nonlocal exchange corrections and Perdew's[31,32] nonlocal correlation correction. The spin-restricted formalism was used for all calculations. Geometries were optimized *without* including nonlocal corrections. In a previous publication, we have shown that in systems such as the one under investigation here the energetics derived by such a procedure deviate by less than 10 kJ/mol from energetics obtained by nonlocal geometry optimization.[33] The Becke−Perdew nonlocal density functional was recently shown to yield barriers which are generally slightly smaller than the experimental values by about 13 kJ/mol.[34,35] All saddle point determinations were initialized by a linear transit search from reactant to product along an assumed reaction coordinate where all degrees of freedom were optimized except for the reaction coordinate which was frozen for each step. Transition states were fully optimized and validated by a frequency calculation where the backbone (Cp, silane, and amido groups) of the constrained geometry catalyst was frozen. Such a constrained frequency calculation neglects modes that couple the intrinsic vibrations of the backbone to the rest of the molecule. However, in this case, it is justified since the geometries of the backbones in all of the optimized structures are virtually identical, which strengthens the argument that coupling between modes intrinsic to the frozen backbone and the "active" part of the molecule is weak. The calculation of free energies followed standard textbook procedures.[36] and were based on the aforementioned constrained frequency calculations.

All reported molecular dynamics simulations were carried out with the Car−Parrinello projector augmented wave (CP-PAW) code developed by Blöchl.[37] The wave function was expanded in plane waves up to an energy cutoff of 30 Ry. The frozen core approximation has been employed. An Ar core has been used for Ti, a Ne core for Si, and a He core for the first-row elements. Periodic boundary conditions were used, with a unit cell spanned by the lattice vectors ([0.0 8.5 8.5] [8.5 0.0 8.5] [8.5 8.5 0.0]) (Å). All simulations were performed using the local density approximation in the parametrization of Perdew and Zunger,[38] with gradient corrections due to Becke[30] and Perdew.[31,32] The accuracy of the PAW method for geometries and energetics has been established by Blöchl.[37] To prevent electrostatic interactions between neighboring unit cells, a charge isolation scheme is used.[39] To achieve an evenly distributed thermal excitation, the nuclei were brought to a temperature of 300 K by applying a sequence of 30 sinusoidal pulses, each of which was chosen to raise the temperature by 10 K. Each of the excitation vectors were chosen to be orthogonal to the already excited modes. A temperature of 300 K was maintained for all simulations by a Nosé thermostat,[40,41] which creates a canonical (NVT) ensemble. The fictitious kinetic energy of the electrons was controlled in a similar fashion by a Nosé thermostat.[42] In order to span large portions of configuration space in a minimum of time, the true masses of the nuclei were rescaled to 5.0 (Ti), 2.0 (Si, N, and C), and 1.5 (H) atomic mass units. Together with an integration time step of 7 au. ($\approx$0.17 fs), this choice ensures good energy conservation during the dynamics simulation without computational overhead due to heavy atomic nuclei. Since we do not discuss time-dependent properties and since configurational ensemble averages remain unchanged under a rescaling of the masses, this technique is appropriate. Since the nuclear velocities scale with $m^{-1/2}$ the sampling is sped up by a factor of 1.5−2. Therefore, all reported simulation times are effectively increased by a factor of 1.5−2, so that a 4 ps simulation yields a sampling accuracy of at least a 6 ps simulation. To sample phase space in the vicinity of the transition state, we choose a reaction coordinate (RC) which is kept constrained during the dynamics using SHAKE[43] constraints. It is desirable that the RC has a high projection onto the IRC[44] (intrinsic reaction coordinate). All other degrees of freedom are allowed to evolve naturally in time. By slowly varying the constraint, phase space in the vicinity of the transition state can be sampled dynamically, leading to undisturbed dynamics for all motions which are orthogonal to the RC and to fictitious dynamics along the RC. This "slow-growth" technique allows us to investigate even high-lying transition states. The total scan time chosen was about 20 000 time steps (=3.4 ps real time) for slow-growth simulations. The free energy difference ΔF between two arbitrary points $\lambda = 0$ and $\lambda = 1$ along the reaction coordinate can

---

[20] Woo, T. K.; Margl, P. M.; Blöchl, P. E.; Ziegler, T. *J. Am. Chem. Soc.*, submitted.

[21] Baerends, E. J.; Ellis, D. E.; Ros, P. *Chem. Phys.* **1973**, *2*, 41.

[22] te Velde, G.; Baerends, E. J. *J. Comput. Chem.* **1992**, *99*, 84.

[23] Versluis, L.; Ziegler, T. *J. Chem. Phys.* **1988**, *88*, 322.

[24] Ravenek, W. In *Algorithms and Applications on Vector and Parallel Computers*; te Riele, H. J. J., Dekker, T. J., van de Horst, H. A., Eds.; Elsevier: Amsterdam, The Netherlands, 1987.

[25] Snijders, J. G.; Baerends, E. J.; Vernoijs, P. *At. Nucl. Data Tables* **1982**, *26*, 483.

[26] Vernoijs, P.; Snijders, J. G.; Baerends, E. J. *Slater Type Basis Functions for the Whole Periodic System*. Department of Theoretical Chemistry, Free University: Amsterdam, The Netherlands, 1981.

[27] Baerends, E. J. Ph.D. Thesis, Free University, Amsterdam, The Netherlands, 1975.

[28] Krijn, J.; Baerends, E. J. *Fit Functions in the HFS Method*. Department of Theoretical Chemistry, Free University: Amsterdam, The Netherlands, 1984.

[29] Vosko, S. H.; Wilk, L.; Nusair, M. *Can. J. Phys.* **1980**, *58*, 1200.

[30] Becke, A. *Phys. Rev. A* **1988**, *38*, 3098.

[31] Perdew, J. P. *Phys. Rev. B* **1986**, *33*, 8822.

[32] Perdew, J. P. *Phys. Rev. B* **1986**, *34*, 7406.

[33] Lohrenz, J. C. W.; Woo, T. K.; Ziegler, T. *J. Am. Chem. Soc.* **1995**, *117*, 12793.

[34] Margl, P. M.; Ziegler, T. *J. Am. Chem. Soc.* **1996**, *118*, 7337.

[35] Margl, P. M.; Ziegler, T. *Organometallics* **1996**, in press.

[36] McQuarrie, D. A. *Statistical Thermodynamics*; Harper & Row: New York, 1973.

[37] Blöchl, P. E. *Phys. Rev. B* **1994**, *50*, 17953.

[38] Perdew, J. P.; Zunger, A. *Phys. Rev. B* **1981**, *23*, 5048.

[39] Blöchl, P. E. *J. Chem. Phys.* **1995**, *103*, 7422.

[40] Hoover, W. G. *Phys. Rev. A* **1985**, *31*, 1695.

[41] Nosé, S. *Mol. Phys.* **1984**, *52*, 255.

[42] Blöchl, P. E.; Parrinello, M. *Phys. Rev. B* **1992**, *45*, 9413.

[43] Ryckaert, J.-P.; Ciccotti, G.; Berendsen, H. J. C. *J. Comput. Phys.* **1977**, *23*, 327.

[44] Fukui, K. *Acc. Chem. Res.* **1981**, *14*, 363.

be determined as

$$\Delta F = \int_0^1 \langle \partial E/\partial \lambda \rangle|_{\lambda,T}\, \mathrm{d}\lambda \tag{1}$$

where λ is just a linear parameter representing any path connecting the two points and the integrand is the appropriately scaled averaged force on the RC sampled at constant temperature and λ. ΔF as derived by this formula does not rely on the harmonic approximation that would be used in the standard treatment based on second derivatives of the total energy. Note that it does not, however, include quantum effects. For eq 1 to give correct results, $\langle \delta E/\delta \lambda \rangle$ must be determined at a large number of λ points between 0 and 1. Furthermore, for each λ point, an extensive sampling is required at constant T to determine the proper average $\langle \delta E/\delta \lambda \rangle_{\lambda,T}$. In the "slow growth" limit, λ is scanned continuously so that only a single value of $\delta E/\delta \lambda$ is determined at each value of λ. This method has the advantage of not disrupting the dynamics when the value of λ is changed. The slow-growth method has been previously demonstrated on several elementary reaction steps in organometallic chemistry.[45−47] In the present case, the integral over the force on the constraint cannot be evaluated fully quantitatively because the scan speed applied is too high. It can, however, be efficiently used to locate stationary points along the RC.

3. Results and Discussion

A. Resting State of the Active Complex. With group 4 transition metal bis-Cp catalysts it is generally agreed that the active catalytic species is a cationic metallocene−alkyl complex.[15,48,49] Theoretical calculations of bis-Cp zirconocenes suggest that the initial product of the insertion process, a γ-agostic Zr−alkyl cation, is likely to rearrange to a more stable β-agostic complex, which is considered to be the resting state of that catalyst system.[15] In this Zr−alkyl resting state the β-agostic hydrogen must vacate its coordination site in order to allow for the formation of the C_α−C_{olefin} bond during the insertion of the next monomer. Our calculations[33] show that this rearrangement process in concert with the insertion is the true rate-determining step in the overall propagation cycle. Thus, the conformation of the resting state between monomer insertions is important when considering the full propagation cycle since rearrangements of the alkyl chain to allow for insertion to occur can be nontrivial.

Another important issue concerning the resting state of the active complex involves the inversion of the metal center. In the assumed and well-established Cossée−Arlman mechanism[50−52] for chain propagation, there is an inversion of the metal center associated with each monomer insertion. Scheme 1a illustrates the normal chain of events which results in successive resting states possessing the opposite absolute configuration. This flip-flop mechanism is important in stereospecific α-olefin polymerization since it most satisfyingly accounts for both isotactic and syndiotactic polymerization.[53] If there is an inversion of the metal center in the resting state before insertion takes place, the flip-flop mechanism is disrupted leading to stereoirregularities. The inversion process can take place by movement of the Ti−C_α bond across the meridional Ti−N−Cp centroid plane as illustrated in Scheme 1c. Another process which can result in a disruption of the flip-flop mechanism is known as back-side insertion.[54,55] This process can be viewed as an inversion of the resting state occurring in concert with the complexation of the olefin. In this way, the coordination of the olefin facilitates the shift of the Ti−C_α bond across the meridional Ti−N−Cp centroid plane as shown in Scheme 1b. In both these processes, the absolute configuration is retained between successive resting states.

Scheme 1

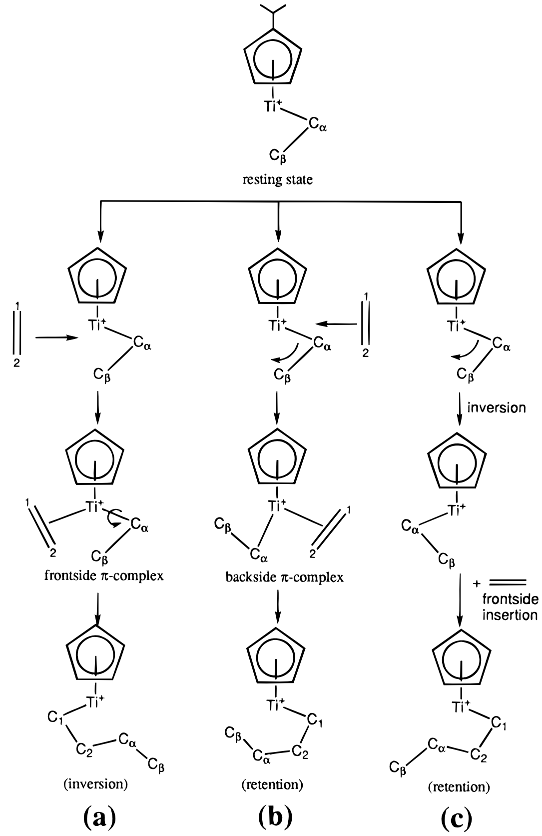

With the intent of studying the resting state structure of the constrained geometry catalysts we performed a Car−Parrinello molecular dynamics simulation of the (CpSiH$_2$NH)Ti−propyl cation. Several theoretical studies of constrained geometry systems have implicated a γ-agostic M−alkyl complex as the kinetic product of the insertion process.[16−18] A propyl group was used as the model growing chain in order investigate the possible rearrangement of the assumed γ-agostic kinetic product of the insertion. A 4 ps (see Computational Details) simulation was performed at 300 K that was initiated from an optimized γ-agostic Ti−propyl cation.

Selected snapshot structures of the simulation are shown in Figure 1 and various structural quantities important in characterizing the resting state are traced in Figure 2. The formation of agostic bonds can be determined by monitoring the Ti−H distances. Figure 2, parts a and b, follow the Ti−H_γ and Ti−H_β distances, respectively, with the shaded regions roughly indicating the formation of agostic bonds. The bold line in

---

(45) Margl, P.; Blöchl, P.; Ziegler, T. *J. Am. Chem. Soc.* **1995**, *117*, 12625.

(46) Margl, P.; Lohrenz, J. C. W.; Blöchl, P.; Ziegler, T. *J. Am. Chem. Soc.* **1996**, *118*, 4434.

(47) Margl, P.; Blöchl, P.; Ziegler, T. *J. Am. Chem. Soc.* **1996**, *118*, 5412.

(48) Jordan, R. F.; Dasher, W. E.; Echols, S. F. *J. Am. Chem. Soc.* **1986**, *108*, 1718.

(49) Yang, X.; Stern, C. L.; Marks, T. J. *Organometallics* **1991**, *10*, 840.

(50) Cossée, P. *J. Catal.* **1964**, *3*, 80.

(51) Arlman, E. J.; Cossee, P. *J. Catal.* **1964**, *3*, 99.

(52) Brookhart, M.; Green, M. L. H. *J. Organomet. Chem.* **1983**, *250*, 395.

(53) It should be noted that there is no requirement for a flip-flop of the growing chain in isospecific α-olefin polymerization. Isospecific polymerization can be explained if the monomer always inserts from the same side as long as the orientation of the monomer remains sincere to the ligand framework and/or chain end. However, the flip-flop mechanism can explain both syndio- and isotactic polymerization since a flip-flop of the growing chain is critical to syndiotactic polymerization.

(54) Fan, L.; Harrison, D.; Deng, L.; Woo, T. K.; Swerhone, D.; Ziegler, T. *Can. J. Chem.* **1995**, *73*, 989.

(55) Lohrenz, J. C. W.; Woo, T. K.; Fan, L.; Ziegler, T. *J. Organomet. Chem.* **1995**, *497*, 91.

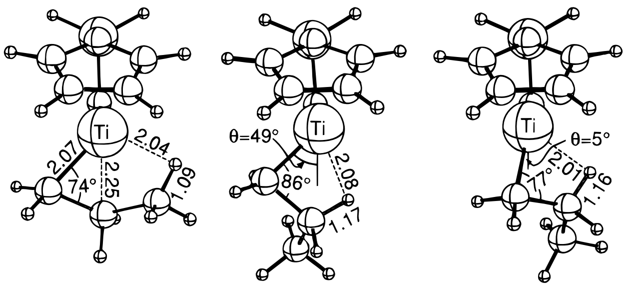

2a **2b** **2c**

Figure 1. Selected γ-agostic (**2a**) and β-agostic (**2b,c**) structures from the Car−Parrinello molecular dynamics simulation of the free Ti−propyl cation. The snapshot structures **2a**−**c** were taken at 2.63, 1.45, and 3.71 ps, respectively. Bond distances are in units of angstroms, and angles are in degrees.

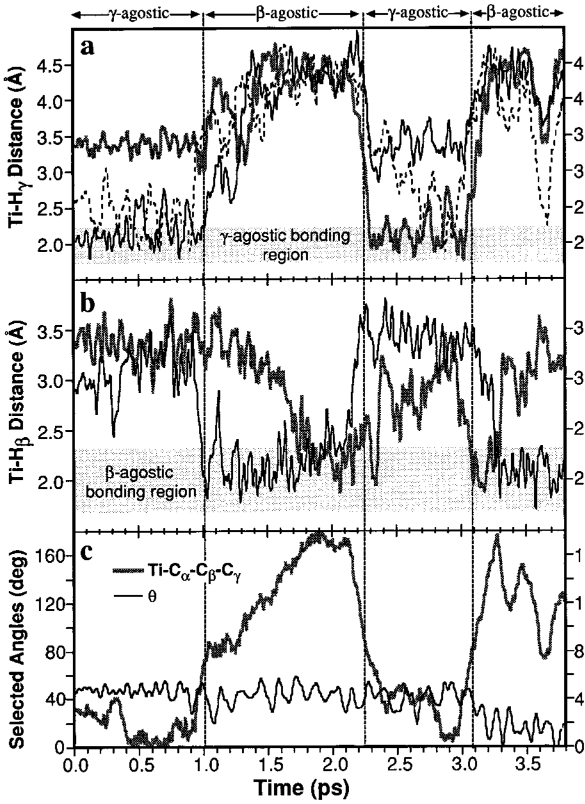

Figure 2. Selected structural quantities as a function of simulation time for a Car−Parrinello molecular dynamics simulation of the free Ti−propyl cation: (a) Ti−H_γ distances; (b) Ti−H_β distances. Shaded regions in a and b indicate agostic bonding. (c) Ti−C_α−C_β−C_γ dihedral angle and the angle θ defined as the angle between the Ti−C_α bond and the meridional Ti−N−Cp centroid plane. Vertical dashed lines separate where the Ti−propyl cation can be characterized as γ-agostic and β-agostic complexes.

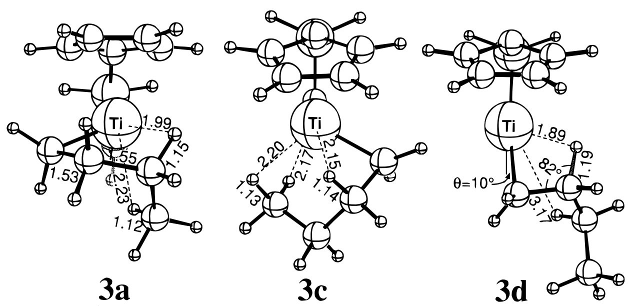

3a (0.0) **3c** (3.7) **3d** (2.0)

Figure 3. Selected optimized Ti−butyl$^+$ complexes. Distances are reported in angstroms and angles in degrees.

Figure 2c traces the Ti−C_α−C_β−C_γ torsion during the simulation. When this torsion is approximately 0° it indicates that the propyl chain is planar, a characteristic of γ-agostic complexation. Conversely, when the torsion is equal to ±120°, it implies β-agostic complexation.

All three indicators, the two Ti−H distances and the Ti−C_α−C_β−C_γ torsion, reveal that the propyl chain rapidly interconverts between the γ- and β-agostic conformations spending roughly equal amounts of time in each conformation. Figure 2a shows that during the time intervals 0.0−1.0 ps and 2.3−3.1 ps at least one and sometimes two Ti−H_γ distances fall in the agostic bonding region of approximately 2 Å. This, along with the small Ti−C_α−C_β−C_γ torsion during these time intervals, signals the formation of a γ-agostic Ti−propyl$^+$ complex. The snapshot structure **2a** taken at 2.63 ps typifies the γ-agostic complexation. In the intervals between 1.0−2.3 and 3.1−3.8 ps, the short Ti−H_β distances indicate the formation of a β-agostic Ti−propyl complex. Structures **2b,c** in Figure 1 are snapshots of the β-agostic complexes in each of these intervals. The dashed vertical lines in Figure 2 separate the regions of γ-agostic complexation and β-agostic complexation. Interestingly, during the course of the simulation, there is always an agostic interaction present. In other words, when a γ-agostic bond was lost, it is immediately replaced by either another γ-agostic bond or a β-agostic bond. This strong preference for the formation of agostic interactions demonstrates the stabilization accrued from these interactions.

The angle between the Ti−C_α bond and the meridional Ti−N−Cp centroid plane, θ, which is plotted in Figure 2c, can be used as an indicator of the inversion process (see Scheme 1). Throughout most of the simulation up to 3.1 ps, the angle fluctuates around 50°, indicating that the Ti−C_α bond is far removed from the meridional plane as in **2a,b**. At a simulation time of approximately 3.1 ps, coincident with the formation of a β-agostic complex, θ steeply decreases to a value of near 10°, indicating that the Ti−C_α bond has moved toward the meridional plane. Structure **2c** is a snapshot of the system at this point and can be characterized as a backside β-agostic Ti−alkyl complex since it is prone to backside coordination of the olefin as depicted in Scheme 1b. The angle θ does not fluctuate between 50° and 10°; instead it remains roughly at either of the two values. This suggests that **2b,c** are distinct structures lying in separate potential wells. Although full inversion of the metal center is not observed, **2c** may be prone to back-side insertion of the monomer.

This CP-MD simulation of a metallocene−alkyl resting state exhibits several interesting features. It shows that for the titanium constrained geometry catalysts there is not a strong preference for the β-agostic structure as there is with the bis-Cp systems.[15,33] The rapid interconversion of one agostic complex to another in the simulation demonstrates the high fluxionality of the alkyl chain in the resting state. It also demonstrates the importance of the agostic bonds in stabilizing the cation since at no point in the simulation is the resting state free of agostic bonding. Finally the simulation shows that the back-side β-agostic complex can readily form.

To complement the CP-MD simulation of the Ti−alkyl resting state, static calculations have been performed wherein the growing chain was modeled[56] by a C_4 chain. Several conformations have been optimized, the most stable of which are shown in Figure 3. The most stable complex **3a** can be characterized as having a strong γ-agostic bond with a weaker δ-agostic bond as evidenced by the short Ti−H_γ and Ti−H_δ

---

(56) A butyl chain was used in order to allow for comparison to our calculations of bis-Cp zirconocenes.[33]

distances of 1.99 and 2.23 Å, respectively. In **3a** the δ-methyl group is oriented toward the amido group. A similar double γ,δ-agostic complex **3b** (not shown) where the δ-methyl group is oriented toward the Cp ring was located 0.8 kJ/mol above **3a**. Also not shown in Figure 3 is a γ-agostic structure **3f** that does not possess an auxiliary δ-agostic interaction as in **3a** or **3b**. This "pure" γ-agostic structure was found to be 14.3 kJ/mol less stable than **3a**. Near in energy to the γ,δ-agostic complex **3a** are two other Ti−butyl conformations, **3c,d**, which are depicted in Figure 3. Compound **3c**, which lies 3.7 kJ/mol above **3a**, is another double agostic complex stabilized by both δ- and β-agostic interactions. Attempts to optimize a pure δ-agostic complex invariably lead to the δ,β-agostic complex **3c**. Complex **3d**, which lies 2.0 kJ/mol above **3a**, can be characterized as a back-side β-agostic complex, analogous to **2c** of the CP-MD simulation. It is noteworthy that **3d** has the shortest Ti−H$_{\text{agostic}}$ distance of all the structures, with a Ti−H$_\beta$ distance of 1.89 Å. Additionally located was a "pure" front-side β-agostic structure, **3e**, similar to **2b**, which is 24.3 kJ/mol less stable than **3a**.

Evidence for agostic interactions is often given by lowered C−H stretching frequencies (100−400 cm^{-1}).[52] In order to confirm that our calculations reproduced this effect, a frequency calculation was performed on structure **3c**, which can be characterized as possessing three agostic hydrogens—two δ-agostic and one β-agostic interaction. Indeed there are three lowered C−H stretching frequencies of 2535, 2609, and 2749 cm^{-1} corresponding to the two δ-agostic and one β-agostic interactions. The remaining CH stretching frequencies ranged from 2832 to 2967 cm^{-1}, as expected[57] for aliphatic $-$CH$_3$ and $-$CH$_2-$ C−H stretching modes.

The large and open active site of the constrained geometry catalyst allows for more than one agostic interaction to stabilize the resting state, and in general, the structures with two agostic stabilizing interactions are the most stable. These calculations suggest that a γ-agostic conformation is the preferred resting state structure, which contrasts similar calculations of bis-Cp metallocenes which show a clear preference for the β-agostic conformation.[33] The calculations also show that there are other low-lying δ,β- and β-agostic conformations close in energy to the preferred γ,δ-agostic Ti−butyl$^+$ complex **3a**, indicating that the resting state of the Ti-constrained geometry catalyst is likely to be very fluxional. This is in good agreement with the MD simulation which demonstrates that the Ti−alkyl cation rapidly interconverts between conformations with different stabilizing agostic interactions. Both the static and dynamic calculations suggest that, to model the approach of an olefin molecule to the Ti−alkyl resting state, at least a propyl group should be used as a model growing chain in order to account for the important γ-agostic conformation. With this in mind we examined the gradual complexation of an olefin molecule to the Ti−butyl resting state.

B. Frontside Coordination of the Monomer to the Ti-Alkyl Cation. We have examined the front-side coordination (Scheme 1a) of an ethene molecule to the preferred γ,δ agostic Ti−butyl complex (**3a**). To explore the olefin coordination, a linear transit calculation was performed in which the C$_\alpha$−olefin midpoint distance was gradually decreased from 9 Å, a distance where the olefin and Ti−alkyl complex are considered to be free and noninteracting. The linear transit calculation reveals that a weakly stabilized γ,δ agostic π-complex (**4a**) shown in Figure 4 forms without barrier. This incipient π-complex is only 13.7 kJ/mol more stable than the free Ti−butyl complex (**3a**) and the free olefin. The weak stabilization is due to the fact that the strong γ- and δ-agostic interactions between the alkyl chain and metal center prevent the formation of a strong π-complex. This is indicated by the long Ti−C$_{\text{olefin}}$ distances in **4a** of 2.67 and 2.63 Å, which can be compared the same distances of 2.44 and 2.39 Å in a (CpSiH$_2$NH)Ti−methyl−olefin$^+$ π-complex optimized at the same level of theory by Fan *et al.*[18] Additionally, the H$_\gamma$−Ti distance elongated only slightly from 1.99 to 2.13 Å and the H$_\delta$−Ti distance in fact decreased from 2.23 to 2.21 Å on going from **3a** to **4a**. By forcing the olefin further into the Ti−C$_\alpha$ bond, a more stable γ-agostic π-complex **4b** is formed which lies 27.1 kJ/mol lower than the incipient π-complex **4a**. In **4b**, the δ-agostic interaction is lost and the γ-agostic interaction is diminished allowing for a stronger π-complex to form in which the Ti−C$_{\text{olefin}}$ distances are 2.42 and 2.51 Å. To compensate for the loss of the δ-agostic stabilization, an α-agostic interaction emerges in **4b** as shown by the short Ti−H$_\alpha$ distance of 2.09 Å. The linear transit calculation indicates that there is a small 8.7 kJ/mol barrier to the isomerization from **4a** to **4b**. Since the linear transit grid was fine, the reported isomerization barrier is a reasonable upper limit for the process. It should be noted that structures **4a,b** are those of the fully minimized complexes where the LT constraint is released.

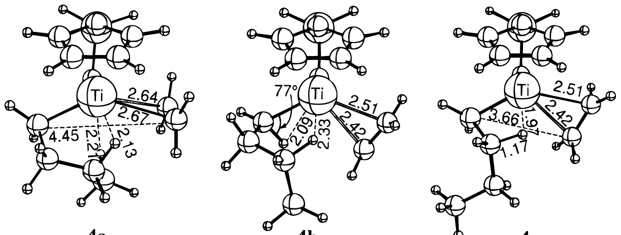

4a (-13.7) **4b** (-40.8) **4c** (-62.8)

Figure 4. Optimized Ti−butyl$^+$ olefin π-complexes. Energies reported are relative to the free Ti−butyl cation and free ethene molecule. Distances are reported in angstroms and angles in degrees.

A β-agostic π-complex **4c** shown in Figure 4 was located 22.0 kJ/mol below **4b** and 49.1 kJ/mol below **4a**.[58] We have determined an approximate isomerization barrier from **4b** to **4c** with a linear transit calculation where the C$_\alpha$−C$_\beta$ bond of the butyl chain was rotated such that the γ-carbon of **4b** moved toward the amido ligand allowing for the formation of a β-agostic bond. A small isomerization barrier of 9.5 kJ/mol was determined, indicating that the γ-agostic π-complexes **4a,b** that may initially form during the course of the insertion are likely to rearrange to a more stable β-agostic π-complex. The insertion of the olefin into the Ti−alkyl bond, therefore, is likely to commence from a β-agostic π-complex. That is, the β-agostic π-complex **4c** represents the lowest minimum before the insertion transition state. To further verify this picture of the coordination process, a CP-MD simulation of the coordination (and subsequent insertion) of the olefin to a γ-agostic Ti−propyl$^+$ complex was performed.

C. Front-Side Insertion. 1. Car−Parrinello Simulation of Frontside Insertion. The slow-growth technique was utilized to study the front-side insertion process with the CP-MD method. A Ti−propyl cation served as the model active complex. The dynamics were initiated from a γ-agostic

---

[57] Silverstein, R. M.; Bassler, G. C.; Morrill, T. C. *Spectrometric Identification of Organic Compounds*, 5th ed.; John Wiley & Sons, Inc.: New York, 1991.

[58] For this process the electronic olefin coordination enthalpy (from **3a** + ethene to **4c**) was determined to be exothermic with $\Delta H_{\text{elec}} = -63$ kJ/mol. It was thought that the olefin coordination would in fact be endergonic at room temperature due to entropic effects. However, for a similar process, the olefin coordination to a Ti-ethyl cation (**10b**), the free energy was negative with $\Delta G = -18$ kJ/mol.

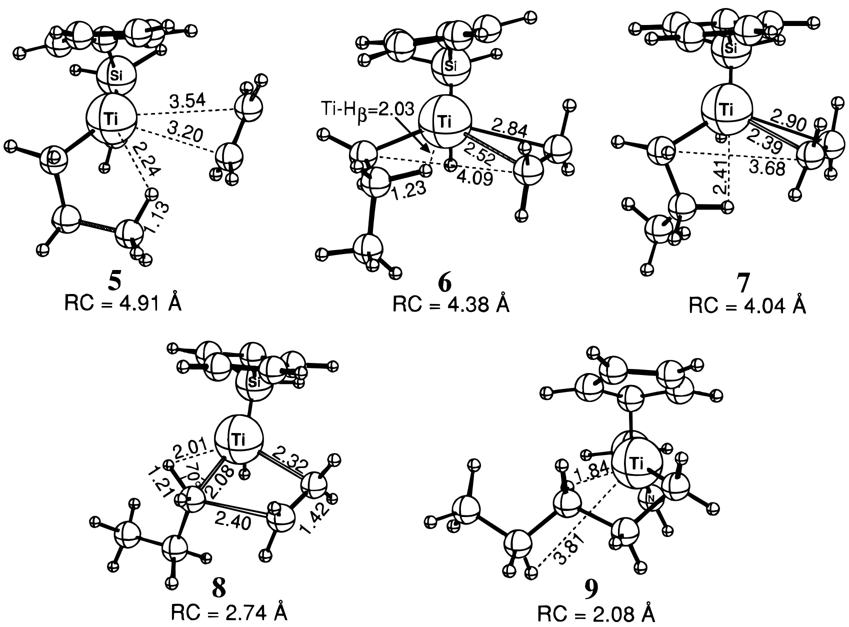

Figure 5. Selected snapshots from the slow growth CP-MD simulation of the front-side insertion. The value below the structure number refers to the value of the reaction coordinate at which the snapshot was taken. Bond distances are in units of angstroms and angles in degrees.

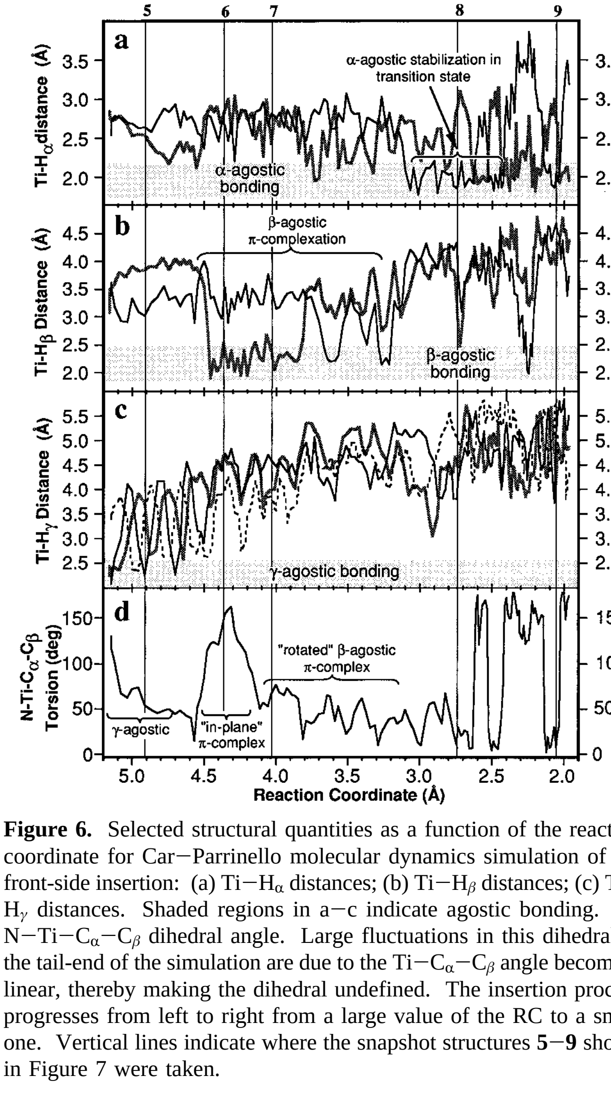

Figure 6. Selected structural quantities as a function of the reaction coordinate for Car−Parrinello molecular dynamics simulation of the front-side insertion: (a) Ti−H$_\alpha$ distances; (b) Ti−H$_\beta$ distances; (c) Ti−H$_\gamma$ distances. Shaded regions in a−c indicate agostic bonding. (d) N−Ti−C$_\alpha$−C$_\beta$ dihedral angle. Large fluctuations in this dihedral in the tail-end of the simulation are due to the Ti−C$_\alpha$−C$_\beta$ angle becoming linear, thereby making the dihedral undefined. The insertion process progresses from left to right from a large value of the RC to a small one. Vertical lines indicate where the snapshot structures **5**−**9** shown in Figure 7 were taken.

conformation of the alkyl chain corresponding to the resting state structure of the growing chain without olefin. The distance between C$_\alpha$ and the midpoint the C−C bond of the ethene molecule was used as the slow-growth reaction coordinate. Previous studies have shown that this is a good RC for this type of process since it has a high projection onto the intrinsic reaction coordinate (IRC).[46,54] In this simulation the RC was varied from a value of 5.1 Å, a distance in which the incoming olefin is too far to form a strong π-complex, to a value of 1.9 Å.

Selected snapshots from the simulation are shown in Figure 5, whereas important structural and energetic quantities monitored as a function of the RC are displayed in Figures 6 and 7, respectively. The Ti−H$_\gamma$ distance as traced in Figure 6c shows that in the initial stage of the simulation the Ti−propyl moiety maintains a γ-agostic conformation until the RC reaches approximately 4.6 Å. A snapshot structure **5** which illustrates the γ-agostic complex in this early stage of the simulation is shown in Figure 5. The large Ti−C$_{olefin}$ distances of 3.5 and 3.2 Å typified in **5** reveal that the π-coordination of the olefin is weak.

Figure 6d which follows the N−Ti−C$_\alpha$−C$_\beta$ torsion indicates how the β-methylene group is oriented. When the dihedral is close to 135°, the β-methylene group lies midway between the Cp centroid and the amido N atom. In this way, the vector which bisects the N−Ti−Cp centroid angle is coplanar with the Ti−C$_\alpha$−C$_\beta$ plane. This is termed the "in-plane" orientation of the β-methylene group. When the torsion is small (near 20°), the β-methylene group is directed toward the amido ligand, and for lack of established terminology, we will term this the "rotated" orientation of the β-methylene group. Torsions greater than 135° indicate that the β-methylene group is directed toward the Cp ligand. In the initial stage of the simulation, the N−Ti−C$_\alpha$−C$_\beta$ torsion steadily drops from its initial value of 130° to a value near 20°, where the RC is 4.6 Å. This movement of the γ-agostic propyl group toward the amido ligand allows for a β-H to form an agostic interaction with the Ti center.

At a RC value of roughly 4.5 Å, a short Ti−H$_\beta$ distance appears (Figure 6b), indicating that the formation of a β-agostic complex which is sustained until a RC value of approximately 3.2 Å. When the initial β-agostic complex is formed, the β-methylene group is rotated toward the amido ligand, but the N−Ti−C$_\alpha$−C$_\beta$ torsion plotted in Figure 6d reveals that the group rapidly moves back toward the Cp ligand to form a more "in-plane" β-agostic complex. This in-plane conformation is

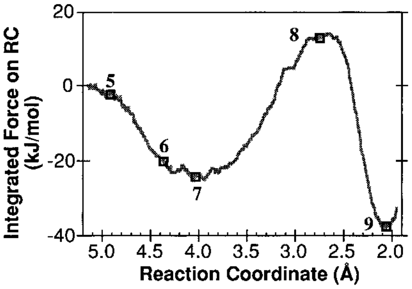

Figure 7. Relative free energy of the system as a function of the slow-growth reaction coordinate as determined from the integrated force on the reaction coordinate. The energetics are qualitative in nature, and therefore, this graph only serves as a guideline to the location important features of the free energy surface. Open squares represent the snapshot structures **5**−**9** shown in Figure 5.

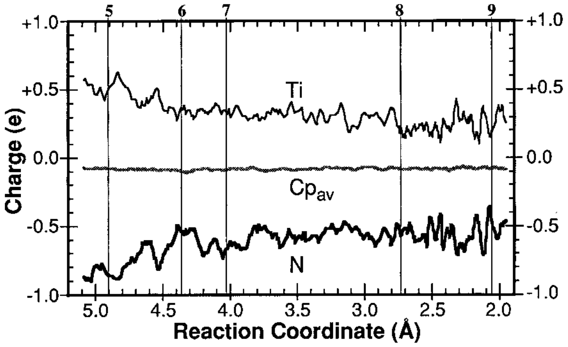

Figure 8. Fitted charges[39] of selected atoms as a function of the reaction coordinate from the Car−Parrinello molecular dynamics simulation of the front-side insertion. Vertical lines indicate where the snapshot structures **5**−**9**.

short lived and passes when the RC is roughly 4.1 Å. Structure **6** of Figure 5, a snapshot of the simulation at a RC value of 4.38 Å, characterizes the coordination in this short period. At this point in the simulation, the Ti−C$_{olefin}$ distances are in the π-bonding regime. For example, in the snapshot structure **6**, the Ti−C$_{olefin}$ distances are 2.5 and 2.8 Å. As expected from previous MD simulations on a similar compound,[46] the olefin moiety is very mobile with respect to rotation around the axis between the metal and the ethylene center-of-mass until a RC of ≈4 Å. Although the time scale of our simulation is distorted due to the fictitious masses of the atoms, it is reasonable to assume that such rotations should in vitro happen with a frequency greater than once per picosecond.

As the coordinated olefin is brought in more tightly, the β-methylene group moves down toward the amido ligand, presumably for steric reasons. This is shown by the drop in the N−Ti−C$_\alpha$−C$_\beta$ torsion which occurs at a RC value of about 4.3 A. A rotated π-complex can be said to form between RC values of 4.1 to 3.2 Å. Structure **7**, which is captured from the simulation at a RC value of 4.04 Å exemplifies, this complexation in this interval.

Plotted in Figure 7 is the integrated force on the reaction coordinate as a function of the RC which can be interpreted as the relative free energy profile for the process (see Computational Details). Because of the limited sampling used, the energetics in this plot should be considered approximate and only used as a rough guide to locate potential wells and transition states in the free energy surface. Figure 7 shows that, from the start of the simulation to where structure **7** lies, there is a steady drop in the free energy of the system. The “rotated” π-complex **7**, lies roughly at a minimum point of the free energy profile. Figure 7 also shows that there is no free energy minimum corresponding to a γ-agostic π-complex as suggested by the static calculations in the previous section. Nevertheless the CP-MD simulation does corroborate the result of the static calculations that the γ-agostic resting state is likely to rearrange during the olefin coordination to form the more stable β-agostic π-complex.

Noteworthy differences between the amido and Cp ligands during the coordination of the olefin can be seen by examining the charges. Plotted in Figure 8 are the fitted charges according to Blöchl[39] on the Ti atom, N atom, and the average of the five Cp C atoms. The Ti atom bears an initial charge of +0.5, which steadily drops to value of approximately +0.3 as the olefin complexes to the Ti−propyl cation. The magnitude of the negative charge on the amido nitrogen atom, correspondingly decreases from an initial value of −0.9 to roughly −0.7 in the π-complex **7**. Interestingly, the average charge on the carbon atoms of the Cp ring remains constant at −0.1 throughout the coordination and subsequent insertion. Thus, electron density is drawn from the amido ligand to stabilize the π-complex by back-donation to the olefin. The Cp ligand in this system does not allow for this. In our work, we found no well-defined potential well corresponding to a olefin π-complex for bis-Cp zirconocenes whereas we did for the Zr constrained geometry catalyst.[16,17] It was postulated that the more open active site of the CGC allowed for formation of a stable π-complex. These results demonstrate that the stability of the CGC π-complex may in actuality be due to the electron-donating ability of the amido ligand. Interestingly, this contrasts the original rationale behind replacing the Cp ring with the amido ligand by Bercaw and co-workers[7] to promote olefin insertion.

Following the formation of the π-complex, as the slow-growth RC is further shortened, the olefin is forced to insert into the Ti−C$_\alpha$ bond. The stabilizing β-agostic interaction is replaced by an α-agostic interaction which begins to intermittently appear at RC = 3.7. As shown by Figure 6a, which follows the two Ti−H$_\alpha$ distances, it is not until the RC reaches 3.1 Å that the α-agostic bonding fully prevails. Analysis of the energetics in Figure 7 reveals that this marks the formation of a transition state structure indicating that there is clear α-agostic assistance in the insertion process. An approximate transition state structure **8**, taken at RC = 2.74 Å, is shown in Figure 5. It is noteworthy that this contrasts the results of the insertion process where the growing chain is modeled by a methyl group. In that case, there was no indication of α-agostic stabilization in the transition state.[18]

The α-agostic interactions which stabilize the transition state correspond to the γ-agostic interactions in the newly formed Ti−pentyl cation when the atoms are relabeled to reflect the new bonding description. The tail end of Figure 6a shows that γ-agostic stabilization is maintained until the end of the simulation. Structure **9**, which lies at the bottom of the free energy well corresponding to the product, is similar to the γ,δ-agostic structure **3a**. The principal difference between **3a** and **9** is that the auxiliary δ-agostic interaction present in **3a** is absent in **9**.

Figure 7 depicts the integral over the force on the RC for the insertion process for the forward scan from the reactants to the product. Since a rapid scanning velocity was used for this slow-growth MD simulation, the free energy differences along the RC provided in Figure 7 are qualitative in nature. As already pointed out in the Computational Details, our simulation conditions were chosen to efficiently locate the preferred insertion pathway as opposed to obtaining high-quality energetics. In order to obtain a better energetic picture of the front-side insertion process, a static simulation of the process was performed.

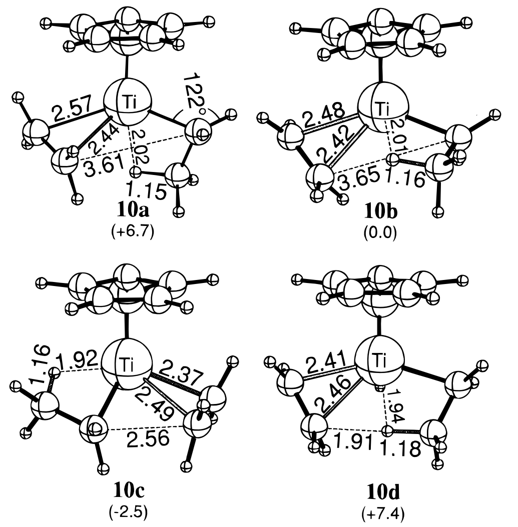

10a (+6.7)

10b (0.0)

10c (-2.5)

10d (+7.4)

Figure 9. Optimized geometries of selected Ti−ethyl$^+$ olefin π-complexes. Energies reported are relative to **10b** in kJ/mol. Distances are reported in angstroms and angles in degrees.

2. Static Simulation of Front-Side Insertion. Both the static and dynamic simulations of the olefin coordination have established that the most favourable olefin π-complex is a β-agostic conformation. Thus, in order to reduce the computational demands of the simulation, an ethyl group was used to model the growing alkyl chain in the static simulation of the insertion process. Commencing from the β-agostic Ti−ethyl$^+$ π-complex the insertion of the olefin results in the formation of the Ti−butyl cation which has been discussed in section 3. This allows us to connect the insertion process and the previously discussed olefin coordination, thus providing for a complete propagation cycle from β-agostic π-complex to β-agostic π-complex.

***π*-Complexes.** Several front-side β-agostic Ti−ethyl$^+$ π-complexes, **10a,b,d**, have been optimized, which are displayed in Figure 9. These complexes are distinguished from one another by the N−Ti−C_α−C_β torsion and the orientation of the ethyl group relative to the olefin moiety. In other words, they are related by a rotation of the ethyl group about the Ti−C_α bond. The most stable of the front-side π-complexes is **10b**. The ethyl group can be characterized as being twisted up toward the Cp ring relative to the coordinated olefin.[59] In **10d** the coordinated olefin and the ethyl group are nearly coplanar. This planar π-complex is 7.4 kJ/mol higher in energy than **10b**. The planar π-complex **10d** can be arrived at from **10b** by rotation of the ethyl group about the Ti−C_α bond such that the ethyl group lies coplanar to the coordinated olefin. Further rotation of the ethyl group toward the amido ligand results in the β-agostic π-complex **10a**, which is 6.7 kJ/mol less stable than **10b**. Compound **10a** is analogous to the snapshot structure **7** of the CP-MD simulation of the olefin insertion described earlier in this section. Further minimas are likely to be found by full rotation of the ethyl group about the Ti−C_α bond, but these were not explored. In addition to the β-agostic complexes, an α-agostic complex was optimized (not shown) which was found to be 22.1 kJ/mol higher in energy than **10b**. This contrasts the situation with bis-Cp zirconocenes, where we found that the difference between analogous β-agostic and α-agostic π-complexes was only 3 kJ/mol.[33]

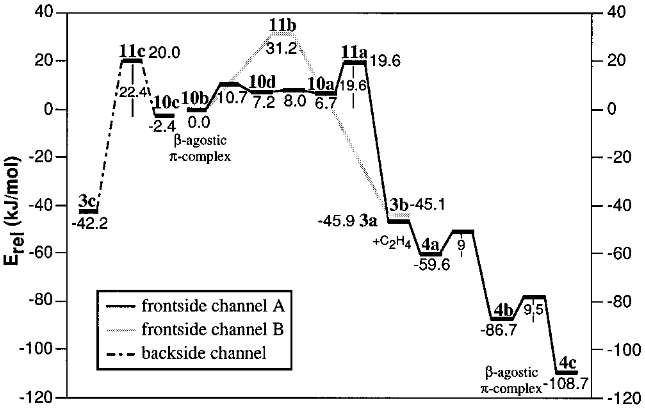

Figure 10. Reaction profiles for front-side and back-side insertion channels. The full propagation profile is presented for the front-side insertion channel A, from β-agostic π-complex to β-agostic π-complex.

The β-agostic Ti−butyl complex **4c** is structurally similar to the β-agostic Ti−ethyl π-complex **10b**. Indeed the Ti−H_β, C_α−C_2, and Ti−C_{olefin} distances in **4c** and **10b** are all within 2% of one another. Even the twist of the alkyl group toward the Cp rings relative to the coordinated olefin in two complexes is alike.[60] The structural similarity between **4c** and **10b** provides further confirmation that the ethyl model for the alkyl chain is a reasonable one in describing the insertion process.

The CP-MD calculations show that a "rotated" π-complex **7**, which is analogous to **10a**, is the preferred front-side π-complex. This contrasts the static calculations which show an electronic preference for the more in-plane complex **10b**. This discrepancy between the dynamics simulation and the static calculations can be accounted for when entropic effects are taken into account. Free energy calculations of the static structures based on a constrained frequency calculation show that **10b** only lies 0.5 kJ/mol below **10a** in free energy at 300 K. At the same time, Figure 7 reveals that the approximate free energy difference between the "rotated" complex **7** and "in-plane" conformation **6** is small and there is no significant free energy barrier separating the conformations. To further explore this we have examined the interconversion processes between the three front-side π-complexes (**10a,b,d**) and found that the barriers are modest. A linear transit calculation was performed connecting **10b** to **10d** and **10d** to **10a** whereby the Ti−C_α bond was rotated. The barrier in converting **10b** to **10d** is 10.7 kJ/mol, and the barrier of converting **10d** to **10a** is only 0.8 kJ/mol. These barriers are displayed in Figure 10 in the initial portion of the solid profile. The small energy differences between the structures and small barriers separating the π-complexes are in reasonable agreement with the MD simulation, suggesting that at room temperature there is rapid interconversion between the structures.

Insertion. Commencing from each of the three front-side π-complexes, the insertion process was explored. Two distinct front-side insertion channels were found, one initiated from the "rotated" π-complex **10a** (channel A) and the other from the π-complex **10b** (channel B).[61] The insertion profiles for the two channels A and B are displayed in Figure 10 as the solid and shaded lines, respectively.

Figure 10 shows that channel A, initiated from the rotated π-complex **10a**, provides a lower energy insertion pathway than

---

(59) This twist of the ethyl group relative to the olefin can be quantified by the angle φ between the Ti−C_α−C_β plane and the Ti−C_{olefin}−C_{olefin} plane, which is 41° for **10b**. In structure **10d**, the ethyl group and the coordinated olefin are nearly coplanar, as illustrated by the small φ angle of 8°. The φ angle is 60° in **10a**.

(60) In **4c** the angle between the Ti−C_α−C_β and Ti−C_{olefin}−C_{olefin} planes is 43° whereas it is 41° in **10b**.

(61) The insertion initiated from the planar π-complex **10c** invariably led first to the formation of the rotated π-complex **10a** and therefore is not a unique insertion channel. Additionally, the insertion was not investigated from the α-agostic π-complex since it was found to lie so much higher than the β-agostic π-complexes.

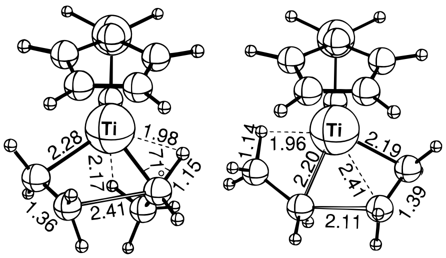

11a **11c**

Figure 11. Optimized transition state for the front-side (**11a**) and back-side insertion (**11c**) process. Distances are reported in angstroms and angles in degrees.

does channel B. The transition state for channel A, **11a** (Figure 11), lies 12.9 kJ/mol above the preceding π-complex **11a**, whereas the transition state for channel B, **11b** (not shown), lies 31.2 kJ/mol above **10b**. The electronic insertion barrier of $\Delta H_{\mathrm{elec}}^{\ddagger} = 12.9$ kJ/mol compares well with our previous estimate[18] of 15.9 kJ/mol whereby the growing chain was modeled by a methyl group. The calculated free energy barrier for the insertion channel A is 24.3 kJ/mol at 300 K, and for channel B, the free energy barrier is 31.9 kJ/mol. The distinguishing feature of the two pathways is how the β-methylene group of the initial π-complex is oriented in the transition state and the product complex. In pathway A, the β-methylene group is oriented toward the amido group, and in channel B, it is oriented toward the Cp ring. In order for the necessary $C_\alpha-C_2$ (see Scheme 1a for atom labeling) bond to form in **10b**, the ethyl group must rotate out of the olefin$-$Ti$-C_\alpha$ plane. Since the ethyl group is twisted toward the Cp ring relative to the coordinated olefin, as the olefin is forced into the Ti$-C_\alpha$ bond, the ethyl group is rotates toward the Cp rings. With channel A the β-methylene group in **10a** is already fully rotated out of the olefin$-$Ti$-C_\alpha$ plane, allowing the C_2-C_α bond to form with less hindrance. As one might expect intuitively, the reaction channel in which the growing chain is directed toward the less bulky ligand is favored. This is in good agreement with the CP-MD simulation of the insertion which exhibits the same orientation of the β-methylene group and which commences from the same rotated π-complex as observed in channel A. Channel A can therefore be said to correspond to the trajectory observed in the dynamics simulation.

The transition states of both insertion channels exhibit clear α-agostic stabilization. This is demonstrated by the short Ti$-H_\alpha$ distances of 1.98 and 2.01 Å in **11a** and **11b**, respectively. This is in good agreement with the CP-MD simulation where the transition state typified by **7** is satisfyingly similar to **11a**. Also, in agreement with the dynamic simulation, the initial β-agostic interactions in the π-complexes **3a,b** are replaced by a stabilizing α-agostic interaction during the course of the insertion process. For example, with channel A, the Ti$-H_\beta$ distance is elongated from 2.02 Å in the π-complex **10a** to 2.17 Å in the corresponding transition state **11a**.

The resulting kinetic products of the two insertion channels A and B are the γ,δ-agostic Ti$-$butyl cations **3a** and **3b**, respectively. Compounds **3a** and **3b** shown in Figure 3 are very similar in both structure and energy with the principal difference between the two being the orientation of the δ-methyl group as discussed earlier in section 3. From the π-complex **10b** to the γ-agostic products, the insertion process is exothermic by 46 kJ/mol. This compares well with the 54 kJ/mol exothermicity when the growing chain is modeled by a methyl group.[18] The γ,δ-agostic Ti$-$butyl complex **3a** provides the link between the insertion profile described here and the olefin coordination described in the previous section. By connecting the two profiles at this point, we have the full propagation cycle from the β-agostic Ti$-$ethyl π-complex **10b** to the β-agostic Ti$-$butyl π-complex **4c**.

The static calculations provide the following picture of the full propagation process as outlined in Figure 10. The preferred Ti$-$ethyl$^+$ π-complex **10b** serves as the origin for the cycle. The π-complex **10b** first isomerizes into **10a** via rotation about the Ti$-C_\alpha$ bond. Then beginning from the "rotated" π-complex **10a**, the insertion of the olefin into the Ti$-C_\alpha$ bond takes place, facilitated by the formation of a stabilizing α-agostic interaction as first proposed by Brookhart, Green, and Rooney.[52,62] The α-agostic stabilized insertion has a free energy barrier of 24.3 kJ/mol at 300 K. The resulting product, **3b**, is a Ti$-$butyl complex which is stabilized by a strong γ-agostic interaction and a somewhat weaker δ-agostic interaction. The Ti$-$alkyl$^+$ resting state appears to be rather flexible, readily forming complexes with various combinations of agostic interactions. Front-side coordination of the next olefin monomer is likely to recover the stable β-agostic π-complex (**4c**), although it may pass through other π-complexes such as the γ-agostic π-complexes **4a,b**. This picture of the front-side insertion process is entirely consistent with the CP-MD simulations which exhibit the same general characteristics.

Our studies show that the propagation processes for the Ti CGC system and the bis-Cp metallocenes are notably different. For bis-Cp zirconocenes it was concluded[33] that the propagation barrier corresponds to a rearrangement process prior to the insertion, whereas this study suggests that the propagation barrier for the Ti CGC system does indeed correspond to the insertion process. Furthermore, the free energy barrier of propagation for the Ti CGC system is calculated to be larger than that of bis-Cp zirconocenes, suggesting that the polymerization activity of the Ti CGC system should be less than that of bis-Cp zirconocene system.

D. Backside Insertion. The static and dynamic calculations of the Ti$-$alkyl$^+$ resting state suggest that the Ti-constrained geometry catalyst can readily adopt a β-agostic conformation (*cf.* **2c** and **3d**) which is inclined to form a back-side olefin π-complex and therefore prone to stereoerrors resulting from a disruption of the flip-flop mechanism.[63] We have performed an exploration of the back-side insertion process as depicted in Scheme 1b with conventional static calculations.

The calculated back-side insertion profile is shown in Figure 10 as the dashed line. A back-side π-complex **10c** was located 2.5 kJ/mol below the front-side π-complex **10b**. The slight preference for the back-side π-complex over the front-side complex is consistent with our calculations of other bis-Cp metallocene systems.[33,46] The transition state structure which lies 22.4 kJ/mol above the back-side π-complex **10c** and 20.0 kJ/mol above the front-side π-complex **10b** is displayed in Figure 11. The free energy barrier commencing from the back-side π-complex **10c** was determined to be $\Delta G^{\ddagger} = 24.8$ kJ/mol. The coplanarity of the olefin moiety and the ethyl group in the π-complex **10c** is maintained through to the transition state, **11c**, where the $C_1-C_2-C_\alpha-C_\beta$ dihedral angle is $-16°$ (see Scheme 1 for atom labeling). However, as the product forms, the resultant butyl chain twists such that the same dihedral in the product Ti$-$butyl complex **3c** is $-67°$. This twist of the butyl chain in the product allows for the formation of a stabilizing β-agostic interaction in addition to the δ-agostic interaction that is maintained throughout the reaction. From the back-side

---

(62) Laverty, D. T.; Rooney, J. J. *J. Chem. Soc., Faraday Trans. 1* **1983**, *1983*, 869.

(63) CGC systems suitable for producing stereospecific polypropylene have been described. (Exxon, European Pat. 420436, 1991.)

β-agostic π-complex **10c** to the δ,β-agostic product the insertion process is exothermic by 39.8 kJ/mol.

The free energy barrier for the front-side and back-side insertion processes are roughly equal. This suggests that the two processes are competitive and that the Ti-constrained geometry catalyst may be prone to stereochemical errors in stereoselective α-olefin polymerization. This issue will be addressed in more detail in future studies of the system.

4. Conclusions

In the present study we have examined the resting state structure of the metallocene alkyl cation and the whole propagation cycle for the Ti-constrained geometry catalyst, $(CpSiH_2NH)TiR^+$, where R = ethyl and propyl. We have utilized a method that combines static DFT calculations[64] with Car–Parrinello molecular dynamics[37,65] simulations at 300 K. From this combined static and dynamic study the following conclusions can be drawn: (i) The $Ti-alkyl^+$ resting state rapidly interconverts between conformations with a variety of agostic interactions. (ii) A γ-agostic $Ti-alkyl^+$ structure is the preferred resting state. (iii) Front-side coordination of the olefin which may initially form γ-agostic π-complexes is likely to lead to the formation of the preferred β-agostic π-complex. (iv) The insertion proceeds through a transition state which is stabilized by α-agostic interactions which replace the β-agostic interactions in the preceding π-complexes. This is different than when the growing chain is modeled by a methyl group which exhibits no α-agostic interactions in the transition state. (v) The overall propagation barrier is the insertion process which is calculated have a free energy barrier of $\Delta G^{\ddagger} = 24.3$ kJ/mol at 300 K. (vi) Calculations show that the back-side insertion process may be competitive with the front-side insertion process.

In this study we have not modeled the effect of the solvent or the counterion which may well play an important role in the chemistry of the catalyst system. If the counterion is closely bound to the Ti center, then the active site may be partially blocked and therefore reduced in size. This situation could sterically favor the more compact intermediates such as the β-agostic $Ti-alkyl^+$ resting state (over the γ-agostic resting state). In a like manner, we have neglected the potential steric importance of what is generally a bulky alkyl substituent on the amido group by modeling it with a hydrogen atom. Again, such a bulky group may interfere with the some of intermediates which we have observed in our simulations. Despite the neglect of these effects this study does provide a good picture of coordination and insertion process for the Ti CGC system. In the second part of this study[20] we examine several chain termination processes and long chain branching mechanisms for this constrained geometry catalyst system.

Acknowledgment. This investigation was supported by the Natural Science and Engineering Research Council of Canada (NSERC), as well as by the donors of the Petroleum Research Fund, administered by the Americal Chemical Society (ACS-PRF No. 31205-AC3). The authors are greatly indebted to Dr. D. Harrison and Dr. J. McMeeking of Novacor Research and Technology (Calgary) for the interesting discussions. We also thank Prof. W. Piers for reading the manuscript and Dr. R. J. Meier for making available to us a preprint of his work. J.C.W.L. thanks the Fond der Chemischen Industrie, who supported this work with a Liebig Stipendium. P.M.M. thanks the Austrian Fonds zur Förderung der wissenchaftlichen Forschung (FWF) for financial support within Project JO1099-CHE. T.K.W. thanks NSERC, the Alberta Heritage Scholarship Fund, and the Izaak Walton Killam memorial foundation.

Supporting Information Available: Quicktime movies of the molecular dynamics simulations presented here on the Internet only. See any current masthead page for Internet access instructions.

JA962525Q

---

(64) Ziegler, T. *Chem. Rev.* **1991**, *91*, 651.

(65) Car, R.; Parrinello, M. *Phys. Rev. Lett.* **1985**, *55*, 2471.